

Diffractive Photoproduction of Jets with a Direct Pomeron Coupling at HERA

B.A. Kniehl^{*,†} H.-G. Kohrs[‡] and G. Kramer

II. Institut für Theoretische Physik[§] Universität Hamburg

Luruper Chaussee 149, 22761 Hamburg, Germany

Abstract

We investigate in detail the effect of a direct pomeron coupling to quarks on the production of jets in ep scattering with almost real photons. Jet production via a direct pomeron coupling is compared with the resolved-pomeron mechanism. We consider both direct and resolved photoproduction. Rapidity and transverse momentum distributions are calculated and compared with preliminary H1 and ZEUS data.

*Present Address: KEK Theory Group, 1-1 Oho, Ibaraki-ken, Tsukuba 305, Japan; address after 1 October 1994: Max-Planck-Institut für Physik, Föhringer Ring 6, 80805 Munich, Germany.

†Supported by Japan Society for the Promotion of Science (JSPS) through Fellowship No. S94159.

‡Supported by Deutsche Forschungsgemeinschaft (DFG) through Graduiertenkolleg.

§Supported by Bundesministerium für Forschung und Technologie (BMFT), Bonn, Germany, under Contract 05 6 HH 93P (5) and by EEC Program *Human Capital and Mobility* through Network *Physics at High Energy Colliders* under Contract CHRX-CT93-0357 (DG12 COMA).

1 Introduction

The production of high-transverse-momentum jets by quasi-real photons on protons is one of the major processes to gain further insight into the interactions of photons with quarks and gluons. Experimental results by the H1 [1] and ZEUS [2] Collaborations at HERA have been presented, and more and better data are expected to come out soon. A subsample of these events are so-called *large-rapidity-gap events*, which have been discovered recently in photoproduction and deep-inelastic electroproduction in both HERA experiments [3, 4]. Their properties were found to be inconsistent with the dominant dynamical mechanism for the production of jets in photoproduction and deep-inelastic electroproduction, where colour is transferred between the produced quark and gluon jets and the proton remnant. Whereas the majority of the events clustered around $\eta_{max} = 4$, a second class of events, with $\eta_{max} \leq 1.5$, were observed, i.e., they had a large gap in rapidity between the fast moving proton, which in the moment is still an assumption, and the rest of the hadronic final state. (Here, η is the rapidity measured along the incoming-proton direction in the laboratory frame.) The same type of events had been observed already some time ago in $p\bar{p}$ scattering [5]. They were interpreted as being due to diffractive hard scattering, following a suggestion of Ingelman and Schlein [6]. In this interpretation, which also applies to the large-rapidity-gap events at HERA, the proton emits a pomeron which acts as a virtual target for the incoming hadron (in the case of $p\bar{p}$ scattering) and the quasi-real or highly virtual photon (in the case of ep scattering), respectively. The incoming proton stays intact or becomes a low-mass state, so that there is no colour flow from the proton to the other final state particles.

Similarly to ordinary hadrons, mesons and baryons, the incoming pomeron is supposed to have a quark and/or a gluon structure, which is probed through electroweak or strong hard-scattering processes and expressed by a pomeron structure function. Models based on different assumptions concerning this quark-gluon structure have been used for calculations of $p\bar{p}$ and ep scattering processes (see, e.g., [7, 8]). Based on these models, Bruni and Ingelman have developed a Monte Carlo program [9] to study the event characteristics, which is

already widely used by the HERA collaborations to interpret their large-rapidity-gap data. If this interpretation is valid, a major task is to disentangle the quark and gluon distributions of the pomeron. As is the case in usual hard-scattering processes, one process is not sufficient to isolate the various parton densities. Several processes must be considered simultaneously. Deep-inelastic diffractive ep scattering primarily measures the quark distribution of the pomeron, while the gluon structure function appears as a higher-order QCD correction. Photoproduction of jets, however, is sensitive to both the quark and gluon densities already in the leading order (LO) of QCD. In LO, photoproduction has two components: a direct one and a resolved one. The latter mechanism has similar features as jet production in diffractive hadron-hadron scattering. The hadron structure function is just replaced by the photon structure function. All these processes can be studied in detail with the Monte Carlo program cited above.

Recently, a number of authors advocated the notion of a direct pomeron coupling to quarks and gluons [10, 11, 12]. Donnachie and Landshoff developed a model in which two gluons emitted coherently from the proton couple to the quark-antiquark system produced by the incoming real or virtual photon [10]. The quark and antiquark thus give rise to two jets associated with the hard scattering. Such configurations give a delta function in the pomeron structure function in the same way as direct photoproduction is equivalent to a delta-function term in the photon structure function of resolved photoproduction. Since in the Donnachie-Landshoff model the second gluon of the pomeron is attached directly to the hard scattering, or to an outgoing parton, the result is higher twist, i.e., considered as a function of p_T , it falls off more strongly than in the case of a factorizable direct pomeron coupling. Subsequently, several groups [11, 12] suggested other mechanisms which break the usual parton-model factorization and are effectively proportional to a delta-function term. These mechanisms, called *coherent hard diffraction* [13] or *lossless diffractive jet production* [12], have the property that the total incoming longitudinal momentum of the pomeron is delivered to the jet system. Both mechanisms produce leading-twist contributions and are not present in deep-inelastic electron-proton scattering, i.e., in quasi-real photoproduction, which we are interested in here primarily, they would occur only in the resolved process. In addition, it is said explicitly that the CFS mechanism [11] leads to a delta-function term

only in the gluon density of the pomeron.

So, these mechanisms for creating a quasi-direct pomeron coupling are very special and their validity is very difficult to assess. They are just conjectures and not proven consequences of QCD. Under these circumstances, it is a challenge to look at experimental data in the diffractive region and to investigate whether such a direct pomeron coupling is present. To that end, it is necessary to establish features which are characteristic for a direct pomeron coupling to quarks and/or gluons in the data. This is the purpose of this work.

In section 2, we formulate the model and give the relevant formulas for calculating the cross section for the production of jets in ep scattering with almost real photons. There, we specify the structure functions of the photon and the pomeron and write down the expression for the pomeron flux. If a direct pomeron coupling exists, this has also consequences for the diffractive contribution of the deep-inelastic structure function F_2 , which in retrospect modifies the input for the photoproduction cross section. In section 3, we present numerical results for the three scenarios: (i) resolved pomeron, (ii) resolved and direct pomeron, (iii) resolved and direct pomeron plus point-like component in the pomeron structure function. The last section is reserved for the conclusions and some outlook to future work.

2 Model for diffractive jet production

The cross section for the diffractive ep scattering process, depicted in Fig. 1, is obtained from the following parton model formula:

$$\begin{aligned}
& \frac{d^3\sigma}{dy d^2p_T}(ep \rightarrow jet + X) \\
&= \sum_{a,b,c,d} \int dx_\gamma G_{\gamma/e}(x_\gamma) \int dx_a G_{a/\gamma}(x_a) \int dx_{\mathbb{P}} G_{\mathbb{P}/p}(x_{\mathbb{P}}) \int dx_b G_{b/\mathbb{P}}(x_b) \\
& \quad \times \frac{\hat{s}}{\pi} \frac{d\sigma}{d\hat{t}}(a + b \rightarrow c + d) \delta(\hat{s} + \hat{t} + \hat{u}) \quad , \tag{1}
\end{aligned}$$

where y and p_T are the rapidity and transverse momentum of the jet, respectively. $\hat{s} = (p_a + p_b)^2$, $\hat{t} = (p_a - p_c)^2$ and $\hat{u} = (p_b - p_c)^2$ are the familiar Mandelstam variables for the

partonic 2–2 scattering process $a + b \rightarrow c + d$. $G_{\gamma/e}(x_\gamma)$ stands for the usual Weizsäcker–Williams formula [14], which gives the flux of the quasi–real photons. The exact form will be specified later. $G_{\mathbb{P}/p}(x_{\mathbb{P}})$ is an integral over the pomeron flux factor $f_{\mathbb{P}/p}(x_{\mathbb{P}}, t)$,

$$G_{\mathbb{P}/p}(x_{\mathbb{P}}) = \int_{t_1}^{t_2} dt f_{\mathbb{P}/p}(x_{\mathbb{P}}, t) \quad , \quad (2)$$

where t is the momentum transfer to the proton line. $t_2 = -m_p^2 x_{\mathbb{P}}^2 / (1 - x_{\mathbb{P}})$, with m_p being the proton mass, is the kinematical upper boundary, while t_1 is determined by the experimental conditions. For $f_{\mathbb{P}/p}(x_{\mathbb{P}}, t)$ we use the Ingelman–Schlein ansatz [6, 9, 15],

$$f_{\mathbb{P}/p}(x_{\mathbb{P}}, t) = \frac{d^2\sigma/dx_{\mathbb{P}} dt}{\sigma_{\mathbb{P}p \rightarrow X}} = \frac{1}{\kappa x_{\mathbb{P}}} \left(a e^{\alpha t} + b e^{\beta t} \right) \quad , \quad (3)$$

with the parameters $\kappa = 2.3 \text{ GeV}^2$, $a = 6.38$, $\alpha = 8.0 \text{ GeV}^{-2}$, $b = 0.424$ and $\beta = 3.0 \text{ GeV}^{-2}$, which were obtained by fitting to the data of the diffractive cross section and the pomeron–proton total cross section. Other functional forms of $f_{\mathbb{P}/p}(x_{\mathbb{P}}, t)$ are given in [16, 17]; they are numerically equivalent in the region of small $|t|$, which dominates the diffractive cross section.

For the unknown pomeron structure functions, $G_{b/\mathbb{P}}(x)$, we make the ansatz

$$\begin{aligned} G_{u/\mathbb{P}}(x) &= G_{\bar{u}/\mathbb{P}}(x) = G_{d/\mathbb{P}}(x) = G_{\bar{d}/\mathbb{P}}(x) = \frac{3}{10}(1-x) \quad , \\ G_{s/\mathbb{P}}(x) &= G_{\bar{s}/\mathbb{P}}(x) = \frac{3}{20}(1-x) \quad , \quad G_{c/\mathbb{P}}(x) = G_{\bar{c}/\mathbb{P}}(x) = 0 \quad , \\ G_{g/\mathbb{P}}(x) &= \frac{9}{2}(1-x) \quad . \end{aligned} \quad (4)$$

The gluon component fulfills

$$\int_0^1 dx x G_{g/\mathbb{P}}(x) = \frac{3}{4} \quad , \quad (5)$$

and the quark components have the normalization

$$\sum_{q, \bar{q}} \int_0^1 dx x G_{q/\mathbb{P}}(x) = \frac{1}{4} \quad . \quad (6)$$

The sum of the gluon and quark parts obeys the sum rule

$$\int_0^1 dx x \left(G_{g/\mathbb{P}}(x) + \sum_{q, \bar{q}} G_{q/\mathbb{P}}(x) \right) = 1 \quad , \quad (7)$$

which is usually assumed also by other authors [9]. Since the exchanged pomeron is not a physical particle, there is no rigid justification for this sum rule, although some motivation can be given.

The quark content of the pomeron can be measured in diffractive deep-inelastic ep scattering (DDIS). Preliminary data from the H1 and ZEUS Collaborations exist, which will be used for comparisons later. The gluon content of the pomeron contributes to DDIS through the order α_s process $\gamma g \rightarrow q\bar{q}$ and is therefore suppressed. This means that, in a first approximation, DDIS is determined by the quark and antiquark components of the pomeron structure function. The gluon component enters when the pomeron structure function is evolved to larger Q^2 , which, however, we shall not perform in the crude study presented here.

For the calculation of the photoproduction of jets, we need the hard-scattering cross sections $d\sigma/d\hat{t}$ in (1). We consider four components, DD, DR, RD, RR. The first letter indicates whether the incoming quasi-real photon interacts directly (D) or as a resolved photon (R) with the incoming quarks and gluons. The second letter characterizes the pomeron interaction; D stands for the direct coupling of the pomeron and R for a resolved pomeron described by the structure functions in (4). The resolved-pomeron hard-scattering cross sections are the usual ones. In the case of a direct photon coupling, we have the photon-gluon-fusion ($\gamma g \rightarrow q\bar{q}$) cross section, where a gluon inside the pomeron is struck, and the gluon-Compton ($\gamma q \rightarrow gq$) cross section, where a quark or antiquark is pulled out of the pomeron. For a resolved photon and a resolved pomeron (RR), we have the well known 2-2 quark and gluon scattering cross sections.

For the calculation of the cross sections with a direct pomeron coupling, we restrict ourselves to a direct coupling with quarks (antiquarks) of the form

$$\mathcal{L}_{int} = c \bar{q}(x) \gamma_\mu q(x) \phi^\mu(x) \quad . \quad (8)$$

Here c is the coupling constant. In (8), we assumed that the pomeron, ϕ , couples to quarks like a vector particle. This contradicts the fact that the pomeron behaves like a $C = +1$ exchange, whereas (8) transforms invariantly under C only if ϕ has $C = -1$. It is an old observation, however, that, in soft processes like diffractive scattering, the pomeron couples to quarks effectively rather like an isoscalar photon, i.e., with a constant γ_μ coupling but with a Regge signature factor, which endows it with even C parity [18, 19]. With this ansatz,

Donnachie and Landshoff were able to give a realistic description of all high-energy elastic and diffractive cross sections applying the additive quark model and including less dominant Regge exchanges [16]. Pomeron exchange with the coupling of (8) also correctly predicts the approximate helicity conservation that is observed experimentally.

With such a coupling, we obtain the following hard-scattering cross section of $\gamma IP \rightarrow q\bar{q}$, written in terms of the invariants, \hat{s} , \hat{t} , \hat{u} , introduced earlier:

$$\frac{d\sigma}{d\hat{t}}(\gamma IP \rightarrow q\bar{q}) = \frac{1}{16\pi(\hat{s}-t)^2} 6e^2 e_q^2 c^2 \left(\frac{\hat{u}}{\hat{t}} + \frac{\hat{t}}{\hat{u}} + \frac{2\hat{s}t}{\hat{u}\hat{t}} \right) , \quad (9)$$

where e_q is the electric charge of q in units of the positron charge, e . Here, t is the momentum transfer at the proton vertex: $t = m_P^2$, if the pomeron is timelike with mass m_P , while $t < 0$ in our application. Of course, (9) is identical to the cross section of $\gamma\gamma^* \rightarrow q\bar{q}$, where γ^* is an off-shell photon with momentum squared t .

Introducing the transverse momentum p_T and the rapidity y of the outgoing jet, we have

$$\cosh y = \frac{\sqrt{\hat{s}}}{2p_T} , \quad \hat{u}\hat{t} = \frac{p_T^2}{\hat{s}} (\hat{s}-t)^2 , \quad \hat{u} + \hat{t} = -\hat{s} + t , \quad (10)$$

so that

$$\frac{d\sigma}{dp_T^2}(\gamma IP \rightarrow q\bar{q}) = \frac{1}{16\pi\hat{s}(\hat{s}-t)} \frac{1}{\sqrt{1-4p_T^2/\hat{s}}} 6e^2 e_q^2 c^2 \left[\frac{\hat{s}^2 + \hat{t}^2}{(\hat{s}-t)^2} \frac{\hat{s}}{p_T^2} - 2 \right] . \quad (11)$$

For $\hat{s} \gg p_T^2$, the cross section decreases only like $1/p_T^2$, i.e., it exhibits a rather mild p_T dependence. Furthermore, the rapidity is completely fixed by p_T and \hat{s} . Under the assumption that the pomeron couples like a scalar particle (this would not allow the description of elastic and diffractive scattering proposed in [16]), (11) would only change slightly to

$$\frac{d\sigma}{dp_T^2}(\gamma IP \rightarrow q\bar{q}) = \frac{1}{16\pi\hat{s}(\hat{s}-t)} \frac{1}{\sqrt{1-4p_T^2/\hat{s}}} 6e^2 e_q^2 c^2 \frac{\hat{s}^2 + \hat{t}^2}{(\hat{s}-t)^2} \frac{\hat{s}}{p_T^2} , \quad (12)$$

i.e., for $p_T^2 \ll \hat{s}$ the result coincides with the one for the vector coupling. In the following, we shall assume that the direct pomeron coupling is characterized by (8), i.e., we shall employ (11) for the hard-collision cross section.

In our model for the direct pomeron coupling, the pomeron behaves like a real photon target for $t = 0$. Similarly to $\gamma\gamma$ scattering, the $\gamma IP \rightarrow q\bar{q}$ cross section also contributes to the pomeron structure function, i.e., to deep-inelastic ep scattering. Then the incoming photon in

(11) is off-shell with invariant mass squared ($-Q^2$). In inelastic $e\gamma$ scattering, this represents the contribution of the *point-like* photon in the photon structure function. Similarly, we have a *point-like* contribution to the quark part of the pomeron structure function, which is obtained from (11) by integrating over p_T^2 . In the form of (11), the cross section has a collinear singularity at $p_T = 0$. To remove it, we render the quark masses, m_q , nonvanishing as usual [20] and obtain

$$G_{q/\mathbb{P}}^{pl}(x, Q^2) = \frac{N_c}{8\pi^2} c^2 \left\{ \beta \left[-1 + 8x(1-x) - \frac{4m_q^2}{Q^2} x(1-x) \right] + \left[x^2 + (1-x)^2 + \frac{4m_q^2}{Q^2} x(1-3x) - \frac{8m_q^4}{Q^4} x^2 \right] \ln \frac{1+\beta}{1-\beta} \right\} , \quad (13)$$

with

$$\beta = \sqrt{1 - \frac{4m_q^2 x}{Q^2(1-x)}} .$$

The quark masses are chosen as $m_u = m_d = 0.3 \text{ GeV}$, $m_s = 0.5 \text{ GeV}$ (i.e., equal to the constituent masses) and $m_c = 1.5 \text{ GeV}$. $Q^2 < 0$ is the momentum squared of the off-shell incoming photon. In a more realistic treatment, the mass parameter is replaced by Λ_{QCD} . It is known that (13) is a reasonable approximation for the case of the point-like part of the photon structure function. For large Q^2 , we have

$$G_{q/\mathbb{P}}^{pl}(x, Q^2) = \frac{N_c}{8\pi^2} c^2 \left[x^2 + (1-x)^2 \right] \ln \frac{Q^2(1-x)}{m_q^2 x} . \quad (14)$$

As expected, the point-like part of the quark distribution of the pomeron dominates at large Q^2 . This result is unusual for the structure of such a complicated object as the pomeron. As a first guess, one would expect that the quark distribution function of the pomeron would behave more like the one of a meson, a f or a ρ^o meson say, which is supposed to have no point-like component. Whether this is true can be tested by inspecting the data and trying to eventually place an upper limit on the coupling c . Furthermore, the x dependence of $G_{q/\mathbb{P}}^{pl}(x, Q^2)$ is quite different from the behaviour of the corresponding structure function of a resolved pomeron in (4).

To LO in α_s , only the quark distribution of the pomeron enters into the deep-inelastic $e\mathbb{P}$ structure function $F_2^{\mathbb{P}}(x, Q^2)$, which is

$$F_2^{\mathbb{P}}(x, Q^2) = \sum_q e_q^2 x \left[G_{q/\mathbb{P}}(x) + G_{\bar{q}/\mathbb{P}}(x) + 2 G_{q/\mathbb{P}}^{pl}(x, Q^2) \right] . \quad (15)$$

In Fig. 2, we have plotted the point-like distribution function for the three quark masses $m_q = 0.3, 0.5, 1.5$ GeV and the four values $Q^2 = 2.5^2, 5.0^2, 7.5^2, 10.0^2$ GeV². Notice the logarithmic singularity at $x = 0$. Apart from that, $G_{q/P}^{pl}(x, Q^2)$ falls off with x increasing and increases with Q^2 even at large x , in contrast to what one expects for a hadron-like object. For calculating $G_{q/P}^{pl}$, we have chosen $c = 1$. This value is somewhat smaller than the one deduced from fits to total cross sections and elastic-scattering data by Donnachie and Landshoff [16, 19]. Figure 2d shows the total contribution of the point-like part to $F_2^P(x, Q^2)/(2x)$ for the same Q^2 values, i.e., the sum of the u, d, s, c contributions with the appropriate charge factors. The dents in the curves are caused by the charm threshold.

Under the assumption that factorization is applicable, $F_2^P(x, Q^2)$ can be used to calculate the diffractive contribution to the deep-inelastic structure function $F_2^{diff}(x, Q^2)$ of the proton. The relation is

$$F_2^{diff}(x, Q^2) = \int_x^{x_0} dx_{\mathbb{P}} \int_{t_1}^{t_2} dt f_{\mathbb{P}/p}(x_{\mathbb{P}}, t) F_2^P(x/x_{\mathbb{P}}, Q^2) \quad . \quad (16)$$

Here $f_{\mathbb{P}/p}(x_{\mathbb{P}}, t)$ is the pomeron flux factor given by (3). The diffractive contribution is concentrated at small x , and we shall mostly take $x_0 = 0.01$ as in the experimental analyses by the H1 and ZEUS Collaborations. t_2 is defined below (2), and we choose $t_1 = -1.0$ GeV². The results for $F_2^{diff}(x, Q^2)$ at $Q^2 = 8.5, 15, 30, 60$ GeV² are compared to preliminary H1 data [21] in Fig. 3. We see that the contribution without direct pomeron ($c = 0$) is too small. Of course, this can be changed by increasing $G_{q/P}(x)$ in relation to $G_{g/P}(x)$ in (4); in its present form, the relation is 1:3. With our choice of (4), the agreement with the data is improved significantly when we include the pointlike contribution with $c = 1$. Clearly, Fig. 3 only demonstrates that $c = 1$ is a consistent value for the direct pomeron coupling when the resolved pomeron is described by (4). That our curves for $c = 1$ lie somewhat above the data points can be tolerated, since the data are obtained with the cut $\eta_{max} \leq 1.5$, i.e., only a fraction, presumably not more than 50–70%, of the diffractive contribution is included in the data points. As expected from the cut on the invariant mass M_X , i.e., $x_0 = 0.01$, the data for the diffractive part of F_2 are nonzero only for $x < 10^{-2}$. In the case of $F_2^{diff}(x, Q^2)$, we could, in principle, accommodate a larger value of c by correspondingly scaling down $G_{q/P}(x)$ relative to $G_{g/P}(x)$. By fitting simultaneously $F_2^{diff}(x, Q^2)$ and the jet-photoproduction cross sections to the data, it should be possible to place an upper bound on c .

We emphasize that the proton momentum transfer is neglected in (13) and hence in (15) and in the eP structure function in (16). This is justified, since in (16) the integral over t is dominated by the minimum $|t|$, which is $|t_2| \approx 0$. Of course, it would be worthwhile to consider $F_2^{diff}(x, Q^2)$ in (16) for fixed t and to study the full t dependence.

We now turn to the jet cross sections of diffractive photoproduction. The calculation of the one- and two-jet inclusive cross section is straightforward and proceeds from (1). In this formula, the integration limits must be specified in terms of the external variables. For the one-jet inclusive cross section, they are y , p_T and $S = (p_e + p_p)^2$, the energy squared of the ep centre-of-mass (c.m.) system. For the case of RR, i.e., resolved γ and resolved IP , the incoming parton momenta are $p_a = x_\gamma x_a p_e$ and $p_b = x_P x_b p_p$, so that $\hat{s} = x_\gamma x_a x_P x_b S$, $\hat{t} = -x_\gamma x_a \sqrt{S} p_T e^{-y}$ and $\hat{u} = -x_P x_b \sqrt{S} p_T e^y$ (see Fig. 1). It is clear that all momentum fractions are limited in general to the interval $[0, 1]$. In our formulas, we have chosen the ep c.m. system, and the momentum of the incoming electron is taken along the positive z direction. The transformation to the HERA system will be done when we present the numerical results in the next section. From phase space, we have as the integration limits in (1)

$$\begin{aligned} x_\gamma^{min} &= \frac{e^y}{\frac{\sqrt{S}}{p_T} - e^{-y}} \quad , \quad x_a^{min} = \frac{e^y}{x_\gamma \left(\frac{\sqrt{S}}{p_T} - \frac{e^{-y}}{x_P} \right)} \quad , \\ x_P^{min} &= \frac{e^{-y}}{\frac{\sqrt{S}}{p_T} - \frac{e^y}{x_\gamma}} \quad , \quad x_b^{min} = \frac{e^{-y}}{x_P \left(\frac{\sqrt{S}}{p_T} - \frac{e^y}{x_\gamma x_a} \right)} \quad . \end{aligned} \quad (17)$$

As usual, the functions $G_{i/j}(x_i)$ stand for the probability to find a parton i with momentum fraction x_i in parton j , where i and j may be also the electron, photon or pomeron. $G_{\gamma/e}(x)$ is described by an improved Weizsäcker–Williams function [22]

$$G_{\gamma/e}(x) = \frac{\alpha}{2\pi} \left[\frac{1 + (1-x)^2}{x} \ln \frac{Q_{max}^2}{Q_{min}^2} - \frac{2(1-x)}{x} \right] \quad , \quad (18)$$

where $Q_{max}^2 = 0.01 \text{ GeV}^2$ and $Q_{min}^2 = m_e^2 x^2 / (1-x)$. We adopt the photon structure functions from [23]. The contribution due to a direct photon and a resolved pomeron (DR) is calculated from (1) using $G_{a/\gamma}(x_a) = \delta(1-x_a)$ and the hard-scattering cross sections of $\gamma q \rightarrow gq$ and $\gamma g \rightarrow q\bar{q}$.

Experimentally, the rapidities are limited by $\eta_{max} \leq 1.5$. In the one-jet inclusive cross section, the integration over the rapidity of the second jet goes beyond this limit. To incorporate

the limit, we need to consider the two-jet cross section. It is obtained from

$$\begin{aligned} & \frac{d^3\sigma}{dy_c dy_d dp_T^2}(ep \rightarrow j_c j_d + X) \\ &= \sum_{a,b,c,d} \int_{x_\gamma^{min}}^{x_\gamma^{max}} dx_\gamma G_{\gamma/e}(x_\gamma) \int_{x_P^{min}}^{x_P^{max}} dx_P G_{P/p}(x_P) x_a G_{a/\gamma}(x_a) x_b G_{b/P}(x_b) \frac{d\sigma}{dt}(ab \rightarrow cd) \quad , \end{aligned} \quad (19)$$

where

$$\begin{aligned} x_a &= \frac{p_T}{x_\gamma \sqrt{S}} (e^{y_c} + e^{y_d}) \quad , \\ x_b &= \frac{p_T}{x_P \sqrt{S}} (e^{-y_c} + e^{-y_d}) \quad . \end{aligned} \quad (20)$$

So, for fixed x_γ and x_P , one can directly extract information on the structure functions of the photon and the pomeron by varying p_T , y_c and y_d . The lower limits of the x_γ and x_P integrals are

$$\begin{aligned} x_\gamma^{min} &= \frac{p_T}{\sqrt{S}} (e^{y_c} + e^{y_d}) \quad , \\ x_P^{min} &= \frac{p_T}{\sqrt{S}} (e^{-y_c} + e^{-y_d}) \quad . \end{aligned} \quad (21)$$

Clearly, p_T , y_c and y_d are limited by the conditions $x_\gamma^{min} \leq x_\gamma^{max} \leq 1$ and $x_P^{min} \leq x_P^{max} \leq 1$. The rapidities y_c and y_d are defined in such a way that the incoming electron travels in the positive z direction, i.e., $p_c = p_T(\cosh y_c, 1, 0, \sinh y_c)$ and $p_d = p_T(\cosh y_d, -1, 0, \sinh y_d)$. In the numerical discussion, we shall flip the sign of the rapidity so as to be in conformity with HERA standards. The one-jet inclusive cross section is obtained by identifying $y \equiv y_c$ and integrating (19) over $y_d \in [y_{d1}, y_{d2}]$, where $y_{d1} = -\ln(\sqrt{S}/p_T - e^{-y_c})$ and $y_{d2} = \ln(\sqrt{S}/p_T - e^{y_c})$. In our case, the two-jet cross section is the integral over y_d with the lower limit $y'_{d1} = \max(y_c, y_{d1})$, so that the rapidity gap is always determined by $y = y_c$. In the following, this cross section is denoted by $d^2\sigma(2jet)/dy dp_T^2$, while the inclusive one-jet cross section is called $d^2\sigma(1jet)/dy dp_T^2$.

As the last point, we write down the cross section for the DD process, with direct photon and direct pomeron in the initial state. This amounts to putting $x_a = x_b = 1$ in (1), so that the inclusive one-jet cross section is

$$\frac{d^2\sigma}{dy dp_T^2}(1jet) = \sum_{c,d} \int_{x_\gamma^{min}}^{x_\gamma^{max}} dx_\gamma G_{\gamma/e}(x_\gamma) x_P^2 \frac{\sqrt{S}}{p_T} e^y G_{P/p}(x_P) \frac{d\sigma}{dt}(\gamma IP \rightarrow cd) \quad , \quad (22)$$

where

$$x_{\mathcal{P}} = \frac{e^{-y}}{\frac{\sqrt{S}}{p_T} - \frac{e^y}{x_\gamma}} \quad , \quad (23)$$

i.e., $x_{\mathcal{P}}$ is fixed by y , p_T and x_γ . On the other hand, the condition $x_{\mathcal{P}} \leq x_{\mathcal{P}}^{max}$ determines the lower bound of integration in (22),

$$x_\gamma^{min} = \frac{e^y}{\frac{\sqrt{S}}{p_T} - \frac{e^{-y}}{x_{\mathcal{P}}^{max}}} \quad . \quad (24)$$

In the numerical analysis, we shall exclude x_γ values outside the interval $[0.3, 0.7]$. Then, we shall have $0.3 \leq x_\gamma^{min} \leq x_\gamma^{max} = 0.7$. For fixed p_T , the allowed rapidity interval is fully determined by the condition $x_\gamma^{min} \leq x_\gamma \leq x_\gamma^{max}$.

3 Results

In this section, we present results for the one- and two-jet cross sections as defined in the last section with kinematical constraints as used in the data analyses by H1 and ZEUS. The results are given for the HERA frame with $E_e = 26.7$ GeV, $E_p = 820$ GeV and the positive z axis pointing in the incoming-proton direction. We choose $x_0 = 0.01$ for the upper cut on $x_{\mathcal{P}}$ and use the structure functions for electron, photon and pomeron that were specified in the previous section. Figure 4 shows $d^2\sigma/dy dp_T^2$ for the one-jet inclusive (a-c) and for the two-jet cross section (d-f). The cross sections are plotted as a function of rapidity at $p_T = 5$ GeV. We shall first concentrate on one-jet inclusive production. In Fig. 4a, the direct pomeron coupling, c , is put to zero. Therefore, we have only results for DR and RR. In Fig. 4a, we give also the one-jet inclusive cross section for the usual photoproduction of jets for comparison. As is well known, at $p_T = 5$ GeV, the resolved-photon cross section (R) dominates the direct-photon cross section (D). The diffractive jet cross sections are limited to rapidity values $y \lesssim 1$. (The precise interval will be specified below.) This is due to the x_0 cut or, experimentally, the cut on M_X , the invariant mass of the diffractively produced final state. The DR and RR components have cross sections of the same order. The DR cross section exceeds the RR one at negative rapidities. In Fig. 4b, the direct pomeron coupling is added with $c = 1$. This produces a significant cross section in DD, i.e., with direct photon

and direct pomeron coupling. This cross section is peaked for negative rapidities and is of similar magnitude as the DR component. The RD component is small compared to all others. We emphasize that, at $p_T = 5 \text{ GeV}$, the direct pomeron predominantly contributes together with the *direct photon*.

Figure 4c displays the inclusive one-jet cross sections including also the point-like part of the quark distribution of the pomeron given by (13), again with the normalization $c = 1$. This affects only the DR and RR components. By comparing the respective curves in Figs. 4b, c, we see that the point-like piece of the pomeron structure function leads to a modest increase of these cross sections, by some 10%. This moderate increase is explained by the fact that the gluon structure function of the pomeron is the dominant part in the DR and RR components. In Figs. 4d–f, we repeat the analyses of Figs. 4a–c for the two-jet cross sections. The restriction on the rapidity of the second jet leads to a decrease of the cross sections and limits the rapidity range in the electron direction. In the c.m. frame, the lower edge of the rapidity spectrum now appears at $-\ln(x_\gamma^{\max} \sqrt{S}/2p_T)$, while in the one-jet case it occurs at

$$-\ln \left[\frac{x_\gamma^{\max}}{2} \left(\frac{\sqrt{S}}{p_T} + \sqrt{\frac{S}{p_T^2} - \frac{4}{x_\gamma^{\max} x_P^{\max}}} \right) \right] \approx -\ln \frac{x_\gamma^{\max} \sqrt{S}}{p_T} . \quad (25)$$

In both cases, the upper edge lies at

$$\ln \left[\frac{x_P^{\max}}{2} \left(\frac{\sqrt{S}}{p_T} + \sqrt{\frac{S}{p_T^2} - \frac{4}{x_\gamma^{\max} x_P^{\max}}} \right) \right] \approx \ln \frac{x_P^{\max} \sqrt{S}}{p_T} . \quad (26)$$

The rapidity in the laboratory frame is shifted by $+(1/2) \ln(E_p/E_e)$ relative to the c.m. rapidity. From these results it is obvious that the rapidity distribution for a fixed p_T value near 5 GeV is not useful to distinguish the direct- and resolved-pomeron contributions. The two combinations DD + RD and DR + RR are very similar in their rapidity dependence. Figures 5a, b show the sum over the various components in Fig. 4 for the inclusive one-jet and two-jet cross sections, respectively. In Fig. 5a, we compare our results with recent H1 data [21]. Since these data are given as event rates, we can only compare the shapes. The data point with lowest rapidity is fitted to the theoretical curve, which is in agreement with the other data points within the experimental errors. For simplicity, we choose the normalization factor to be 1/2.

The p_T dependence of the cross sections for fixed rapidity is more discriminative. This can be seen from the results in Fig. 6. In Figs. 6a–c, we have plotted the inclusive one–jet cross section as a function of p_T for fixed $y = 0$, again for the three cases $c = 0$, $c = 1$ and $c = 1$ with point–like pomeron structure function. The DD component has a much slower fall–off in p_T as compared to the DR component and dominates the other components for $p_T \gtrsim 5$ GeV. This harder p_T dependence is expected, since the hard–scattering cross section of $\gamma IP \rightarrow q\bar{q}$ is proportional to $1/p_T^2$. In the DR component, this dependence is softened through the pomeron structure functions. The two–jet cross sections show an almost identical pattern, since the additional restriction for the second jet is less effective, if y is held fixed near the maximum of the rapidity distribution.

The shallow p_T dependence of the DD (and, to a minor extent, of the RD) component is still visible in the sum over all components. This is seen in Figs. 7a, b for the inclusive one–jet and two–jet cross sections, respectively, when we compare the curves for $c = 1$ and $c = 0$. In Figs. 7a, b, we also compare our results with recent H1 [21] and ZEUS data [24], respectively. Similarly to Fig. 5a, we can only compare the shapes. The points with lowest p_T are adjusted so as to match approximately with the theoretical curves, again using a normalization factor of 1/2. The data seem to show the shallow p_T dependence characteristic for the combined direct–pomeron contribution, DD + RD. However, this observation should be taken with a grain of salt. Firstly, these data are uncorrected. Secondly, for a serious comparison, our model should include hadronization, which is certainly important for the low effective c.m. energies in the γIP channel. Therefore, we believe that it is premature to draw any firm conclusions from these comparisons.

There are two other features in the ZEUS data that are indicative of a direct pomeron coupling. The $x_\gamma \equiv x_a$ distribution is peaked near $x_\gamma = 1$, and the x_b distribution, i.e., the dependence on the pomeron–structure–function variable x_b , has also a maximum near $x_b = 1$. But also here, conclusions can be drawn only when corrected data are available and hadronization effects are included in our model.

4 Conclusions and Outlook

In this work, we studied the effect of a direct pomeron coupling to quarks, which leads to lossless diffractive jet production. We considered ep scattering under HERA conditions with almost real photons. We tried to conform to the experimental conditions of the H1 and ZEUS experiments as much as possible. Only LO processes were investigated, and the hadronization of the parton jets was neglected. The most important signature of a direct pomeron coupling is the p_T distribution in inclusive one-jet and two-jet production. It leads to a much flatter p_T distribution than in the case of a resolved pomeron. The direct photon coupling gives the dominant contribution at $p_T \gtrsim 5 \text{ GeV}$. Most of our results are model-dependent, since we have no a-priori knowledge about the strength of the pomeron coupling and about the relation of the quark to the gluon components of the pomeron structure function. We considered the gluon part to be dominant over the quark part in the ratio 3 : 1. So far, the existing preliminary experimental information on jet production with almost real photons in rapidity-gap events observed by H1 and ZEUS is consistent with this assumption. Definite conclusions are not possible at this time, since these data are not yet corrected and our model does not contain hadronization corrections, which are likely to be important at these low energies in the γIP c.m. system.

We are aware of the fact that the assumption of a direct pomeron coupling to quarks is quite unconventional, since the pomeron is a very complex object, which, at first hand, is not expected to behave similarly to a photon. On the other hand, theory cannot guide us. So, only data can tell whether our assumptions are realistic.

There exist several modifications of the ideas presented in this work. Firstly, the direct pomeron coupling to quarks could contain an additional form factor which depends on p_T . In this case, we would expect that the p_T dependence of the DD component is not as flat as in Fig. 6. Therefore, it would be much harder to detect such a direct coupling. Secondly, the direct coupling of the pomeron might be to gluons and not to quarks—or to both. For a direct gluon coupling of the pomeron, the direct-photon contribution does not exist in LO. Therefore, such a coupling could be seen only in connection with a resolved photon.

Of course, for this case, there is also no point-like component in the pomeron structure function. If direct pomeron couplings both to quarks and to gluons exist, it will be difficult to disentangle the two.

It is conceivable that, when the experimental range of x_P can be increased, also other Regge exchanges between the primary proton vertex and the hard-scattering process will become relevant. Such exchanges, like π , ρ , etc., have been considered in the past as a method for extracting the deep-inelastic structure of Reggeons [26] when the incoming photon is highly virtual. Such exchanges are also possible in ep scattering with almost real photons. In this case, a direct π (ρ , etc.) coupling to quarks is even more natural than a direct pomeron coupling to quarks. Actually, in a recent publication [27] by the E-683 Collaboration at Fermilab on jet production by real photons in the fixed-target energy range, it is reported that the energy flow in the photon (forward) direction is very similar in γp and πp reactions at comparable energies. Since γp processes at such low c.m. energies are dominated by *direct* photoproduction, this result can be interpreted by assuming that also the pion has an appreciable direct coupling to quarks, in contrast to naïve expectations.

Similar results were reported earlier by the E-609 Collaboration [28] for hard πp collisions at 200 GeV on a fixed target. These authors found evidence for two-jet events with little or no energy flow in the forward direction. They interpreted these results in terms of a higher-twist process suggested by Berger and Brodsky [29]. In this model, the pion structure function has a delta-function component with a form factor that is related to the electromagnetic form factor of the pion. Except for these higher-twist factors, which reduce the cross section and produce a steeper p_T dependence, the cross section has the same characteristics as the one of jet production in γp collisions with a direct photon.

It is possible that the pomeron, too, has such a higher-twist component. This means that, independently of whether the pomeron model with a leading-twist direct coupling proposed in this work is true or not, it might be reasonable to look for lossless diffractive jet production in ep collisions, which could be a signature for a higher-twist direct coupling. We remark that the c.m. energies in the γp collisions considered in this work are of the same order as those in the πp fixed-target experiments.

ACKNOWLEDGMENTS

We would like to thank G. Wolf for useful comments on the ZEUS data on diffractive photo-production of jets and G. Ingelman for carefully reading the manuscript. One of us (BAK) is indebted to the KEK Theory Group for the warm hospitality extended to him during his visit, when this work was finalized.

References

- [1] T. Ahmed et al., H1 Collaboration, Phys. Lett. **B297** (1992) 205.
- [2] M. Derrick et al., ZEUS Collaboration, Phys. Lett. **B293** (1992) 465.
- [3] M. Derrick et al., ZEUS Collaboration, Phys. Lett. **B315** (1993) 481; Preprint DESY 94-063 (1994).
- [4] J. Dainton, Preprint RAL-94-012 (1994), also in *Proceedings of the XVI International Symposium on Lepton and Photon Interactions*, Ithaca, New York, 1993, edited by P. Drell and D. Rubin (AIP Press, New York, 1994) p. 87; A. De Roeck, H1 Collaboration, Preprint DESY 94-005 (1994), also in *Proceedings of the International Europhysics Conference on High Energy Physics*, Marseille, France, 1993, edited by J. Carr and M. Perrottet (Editions Frontières, Gif-sur-Yvette, 1994) p. 791.
- [5] R. Bonino et al., UA8 Collaboration, Phys. Lett. **B211** (1988) 239; A. Brandt et al., UA8 Collaboration, Phys. Lett. **B297** (1992) 417.
- [6] G. Ingelman and P.E. Schlein, Phys. Lett. **B152** (1985) 256.
- [7] N. Artéaga-Romero, P. Kessler and J. Silva, Mod. Phys. Lett. **A1** (1986) 211; Preprint LPC 86-25 (1986); G. Ingelman, Nucl. Phys. **B** (Proc. Suppl.) 18C (1990) 172; J. Phys. **G19** (1993) 1633.
- [8] K.H. Streng, Preprint CERN-TH-4949 (1988), also in *Proceedings of the Workshop on Physics at HERA*, Hamburg, Germany, 1987, edited by R.D. Peccei, p. 365.

- [9] P. Bruni and G. Ingelman, POMPYT 1.0 (to be published); Preprint DESY 93–187 (1993), also in *Proceedings of the International Europhysics Conference on High Energy Physics*, Marseille, France, 1993, edited by J. Carr and M. Perrottet (Editions Frontières, Gif-sur-Yvette, 1994) p. 595; see also H. Jung, RAPGAP; Preprint DESY 93–182 (1993).
- [10] A. Donnachie and P.V. Landshoff, Phys. Lett. **B285** (1992) 172; see also N.N. Nicolaev and B.G. Zakharov, Z. Phys. **C53** (1992) 331.
- [11] J.C. Collins, L. Frankfurt and M. Strikman, Phys. Lett. **B307** (1993) 161.
- [12] A. Berera and D.E. Soper, Preprint OITS 536 and AZPH–TH/94–02 (1994).
- [13] J.C. Collins, J. Huston, J. Pumplin, H. Weerts and J.J. Whitmore, Preprint CTEQ/PUB/02, FNAL/ and PSU/TH/136 (1994).
- [14] C.F.v. Weizsäcker, Z. Phys. **88** (1934) 612; E.J. Williams, Phys. Rev. **45** (1934) 729.
- [15] G. Ingelman and K. Prytz, Preprint DESY 92–177 (1992); Z. Phys. **C58** (1993) 285.
- [16] A. Donnachie and P.V. Landshoff, Nucl. Phys. **B244** (1984) 322.
- [17] E.L. Berger, J.C. Collins, D.E. Soper and G. Sterman, Nucl. Phys. **B286** (1987) 704.
- [18] P.V. Landshoff and J.C. Polkinghorne, Nucl. Phys. **B32** (1971) 541.
- [19] G.A. Jaroskiewicz and P.V. Landshoff, Phys. Rev. **D10** (1974) 170.
- [20] L.E. Gordon and J.K. Storrow, Z. Phys. **C56** (1992) 307 and references cited therein.
- [21] J. Feltesse, DESY Seminar, March 29, 1994; see also A. de Roeck, DESY Seminar, July 15, 1994.
- [22] A. Rostovtsev and V. Soloshenko, H1 Note H1–08/93–309 (1993).
- [23] M. Glück, E. Reya and A. Vogt, Phys. Rev. **D45** (1992) 3986; Phys. Rev. **D46** (1992) 1973.

- [24] R. Devenish, lecture delivered at the *Mini-School on Diffraction at HERA*, DESY, May 5, 1994; G. Wolf, talk presented at the *International Workshop on Deep Inelastic Scattering (DIS) and Related Subjects*, February 6–11, 1994, Eilat, Israel.
- [25] J. Botts, J.G. Morfin, J.F. Owens, J. Qiu, W.–K. Tung and H. Weerts, CTEQ Collaboration, Phys. Lett. **B304** (1993) 159, now superseded by J. Botts, H.L. Lai, J.G. Morfin, J.F. Owens, J. Qiu and W.–K. Tung, CTEQ2 Collaboration, Preprint MSUHEP–93/28 (1993); K. Charchuła, Comp. Phys. Commun. 69 (1992) 360.
- [26] J.D. Sullivan, Phys. Rev. **D5** (1972) 1732; G. Kramer, in *Proceedings of the Seminar on e–p and e–e Storage Rings*, edited by J.K. Bienlein, I. Dammann and H. Wiedemann, Preprint DESY 73/66 (1973), p. 3; G. Altarelli, N. Cabibbo, L. Maiani and R. Petronzio, Nucl. Phys. **B92** (1975) 413; N.S. Craigie and G. Schierholz, Nucl. Phys. **B100** (1975) 125.
- [27] D. Adams et al., E–683 Collaboration, Phys. Rev. Lett. **72** (1994) 2337.
- [28] C. Naudet et al., E–609 Collaboration, Phys. Rev. Lett. **56** (1986) 808.
- [29] E.L. Berger and S.J. Brodsky, Phys. Rev. **D24** (1981) 2428.

FIGURE CAPTIONS

Figure 1:

Generic diagram for the diffractive ep scattering process with a resolved photon γ , a resolved pomeron IP and the hard subprocess HS .

Figure 2:

The x dependence of the point-like distribution function, $G_{q/IP}^{pl}(x, Q^2)$, for various values of Q^2 and for the three quark masses a) $m_q = 0.3$ GeV, b) $m_q = 0.5$ GeV, c) $m_q = 1.5$ GeV; the e_q^2 -weighted sum, $\sum_q e_q^2 G_{q/IP}^{pl}(x, Q^2)$, where $q = u, d, s, c$, is shown in d).

Figure 3:

$F_2^{diff}(x, Q^2)$ compared to preliminary H1 data. The solid curves represent only the contributions from quarks in the resolved pomeron, while for the dashed lines the point-like contribution with $c = 1$ is included.

Figure 4:

The rapidity distributions of the one-jet [a)–c)] and two-jet [d)–f)] cross sections for fixed $p_T = 5$ GeV in the ep laboratory system. Here y is defined to be positive for jets travelling in the proton direction. Figures a), d) show the non-diffractive cross sections with a direct (D) and resolved (R) photon in comparison with the DR and RR contributions in our model. Due to $c = 0$, there are no DD or RD contributions. In Figs. b), e), these contributions are included for $c = 1$ but without the point-like (pl) component of the pomeron. This contribution is switched on finally in Figs. c), f).

Figure 5:

The y distributions of the a) one-jet and b) two-jet cross sections for fixed transverse momentum $p_T = 5$ GeV after summing up the various contributions shown in Fig. 4. For a direct comparison with data, the one-jet events from H1 with suitable normalization are also shown.

Figure 6:

The p_T spectra of the one-jet [a)–c)] and two-jet [d)–f)] cross sections for fixed rapidity $y = 0$. Figures a)–f) have to be considered in full analogy to Figs. 4a)–f).

Figure 7:

The p_T spectra of the a) one-jet and b) two-jet cross sections for fixed rapidity $y = 0$ after summing up the various contributions shown in Fig. 6. For a direct comparison with data, the one-jet events from H1 and the two-jet events from ZEUS with suitable normalizations are also shown. Like in Figs. 4a), d), we have also plotted the non-diffractive result D+R.

This figure "fig1-1.png" is available in "png" format from:

<http://arxiv.org/ps/hep-ph/9408340v1>

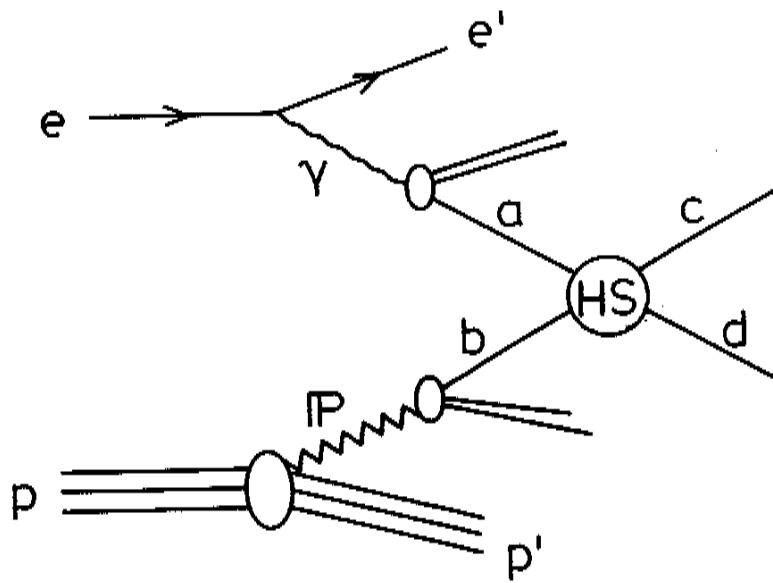


Fig. 1

This figure "fig2-1.png" is available in "png" format from:

<http://arxiv.org/ps/hep-ph/9408340v1>

This figure "fig1-2.png" is available in "png" format from:

<http://arxiv.org/ps/hep-ph/9408340v1>

This figure "fig2-2.png" is available in "png" format from:

<http://arxiv.org/ps/hep-ph/9408340v1>

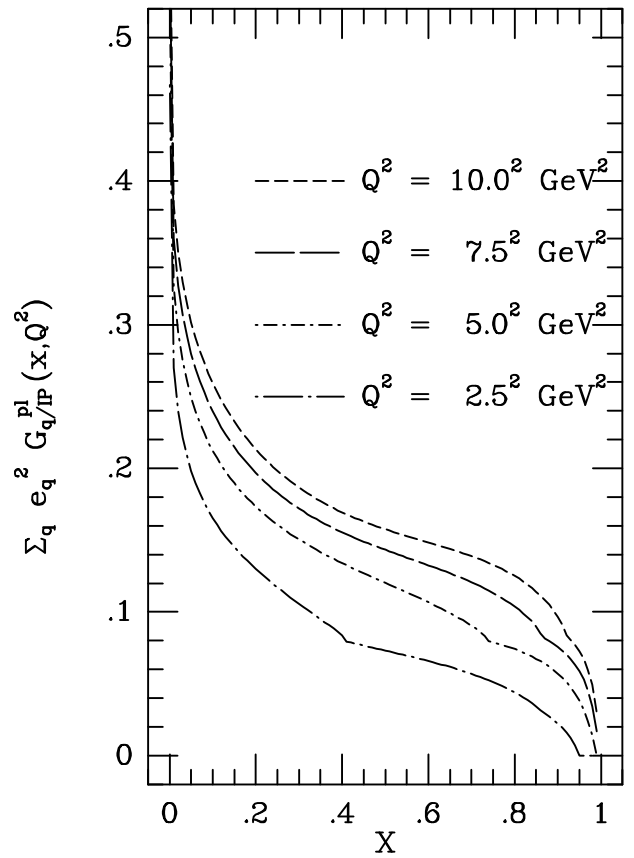
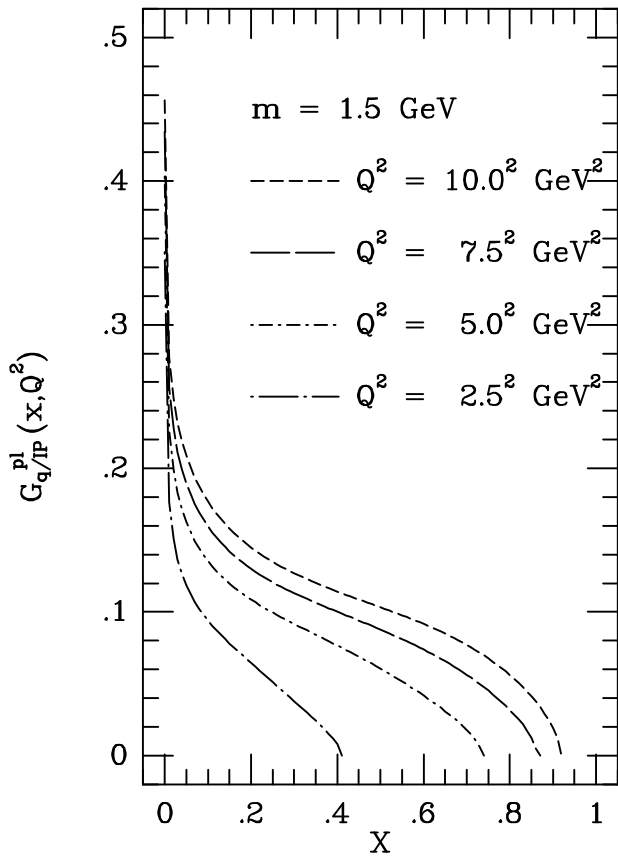
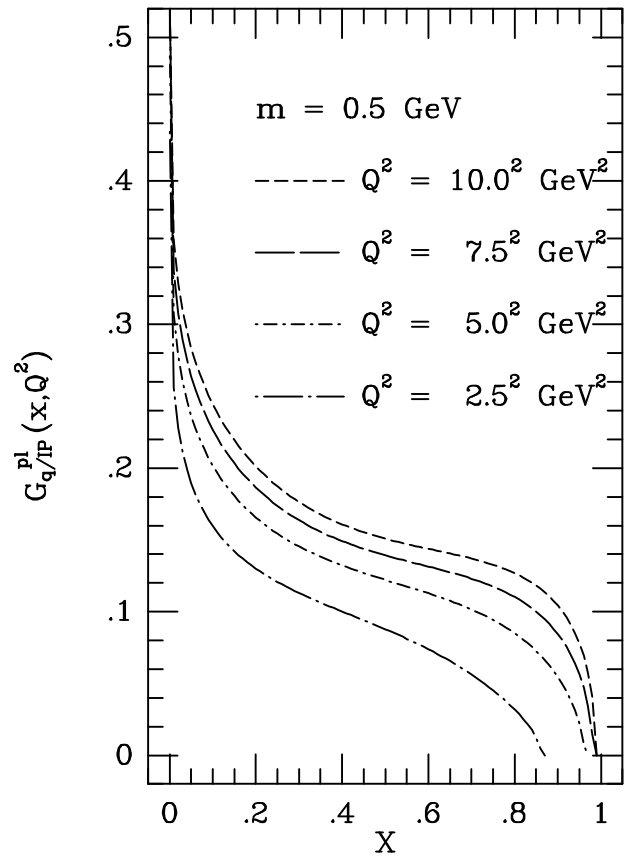
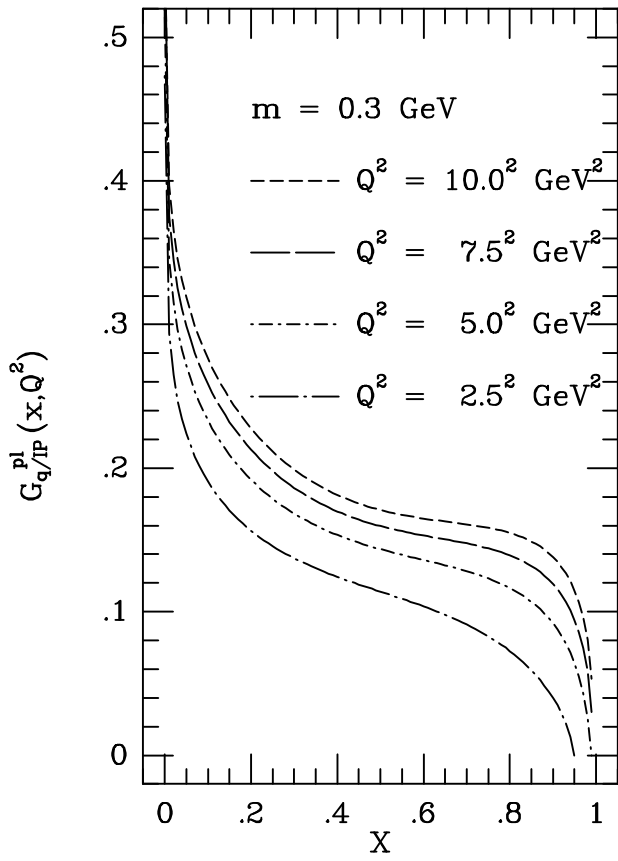


Fig. 2

This figure "fig1-3.png" is available in "png" format from:

<http://arxiv.org/ps/hep-ph/9408340v1>

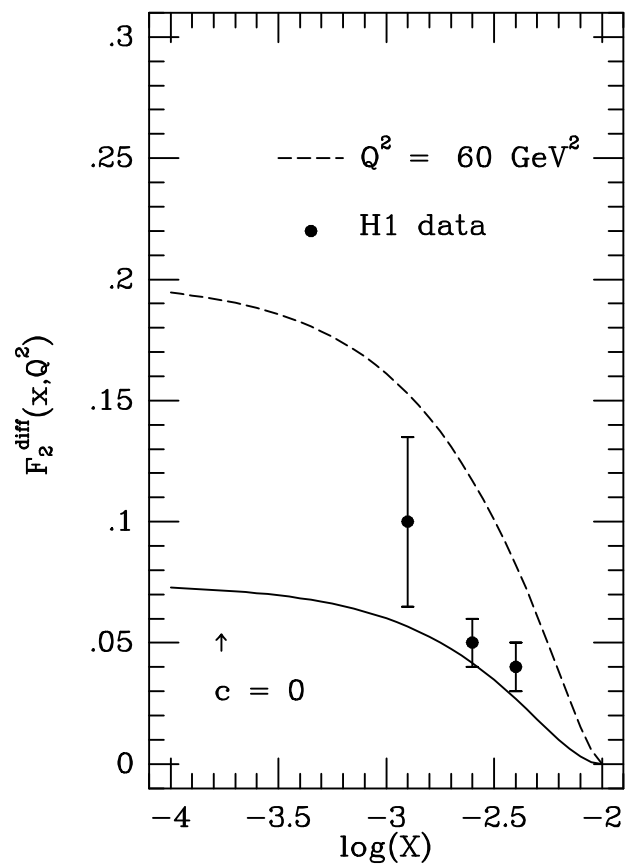
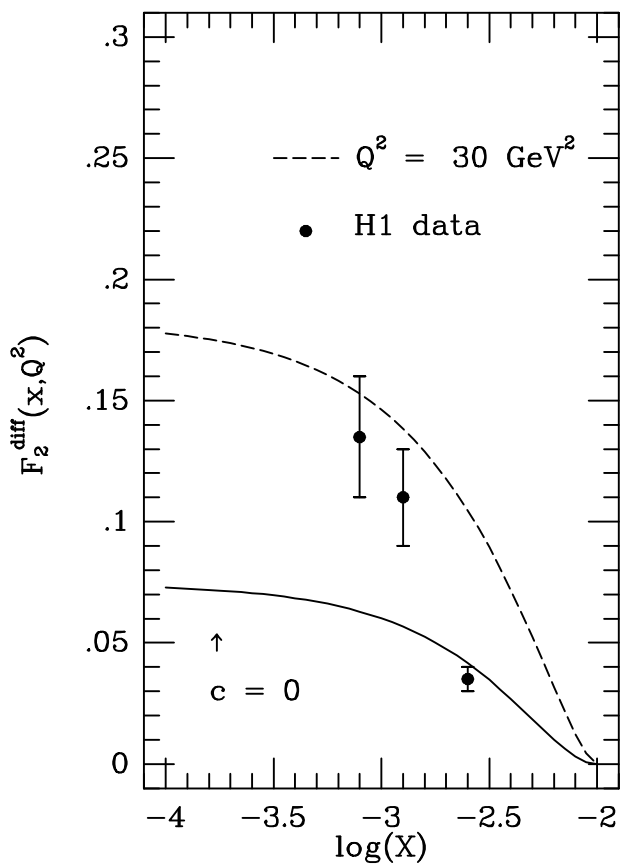
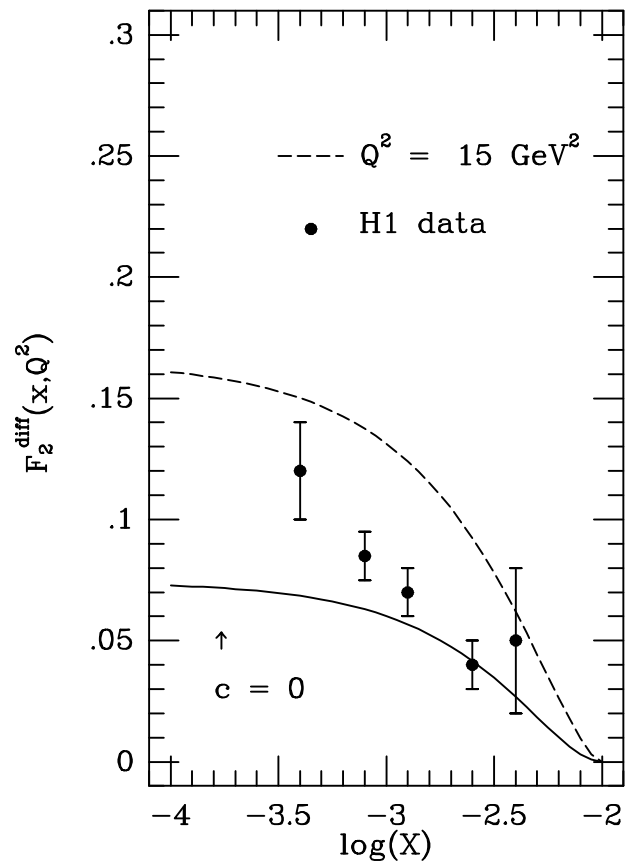
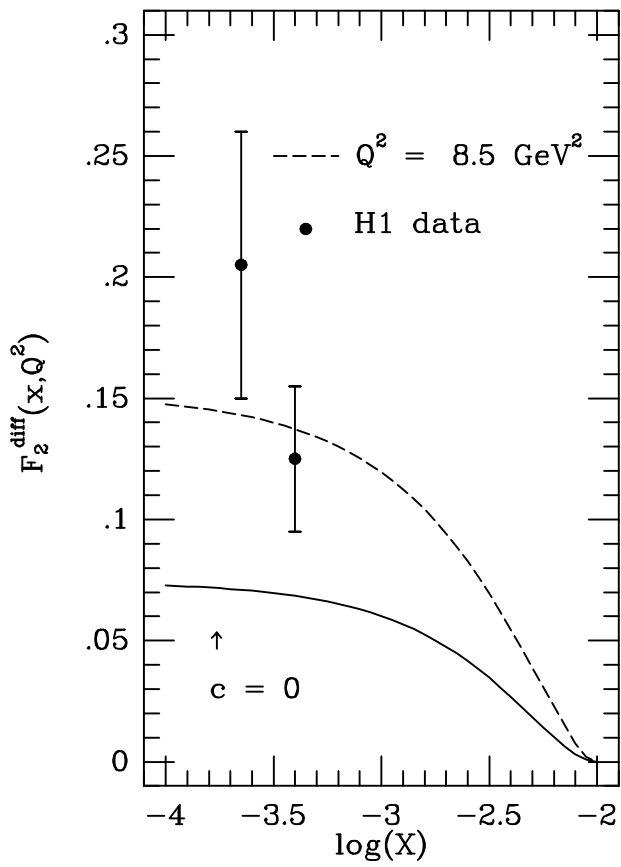


Fig. 3

This figure "fig1-4.png" is available in "png" format from:

<http://arxiv.org/ps/hep-ph/9408340v1>

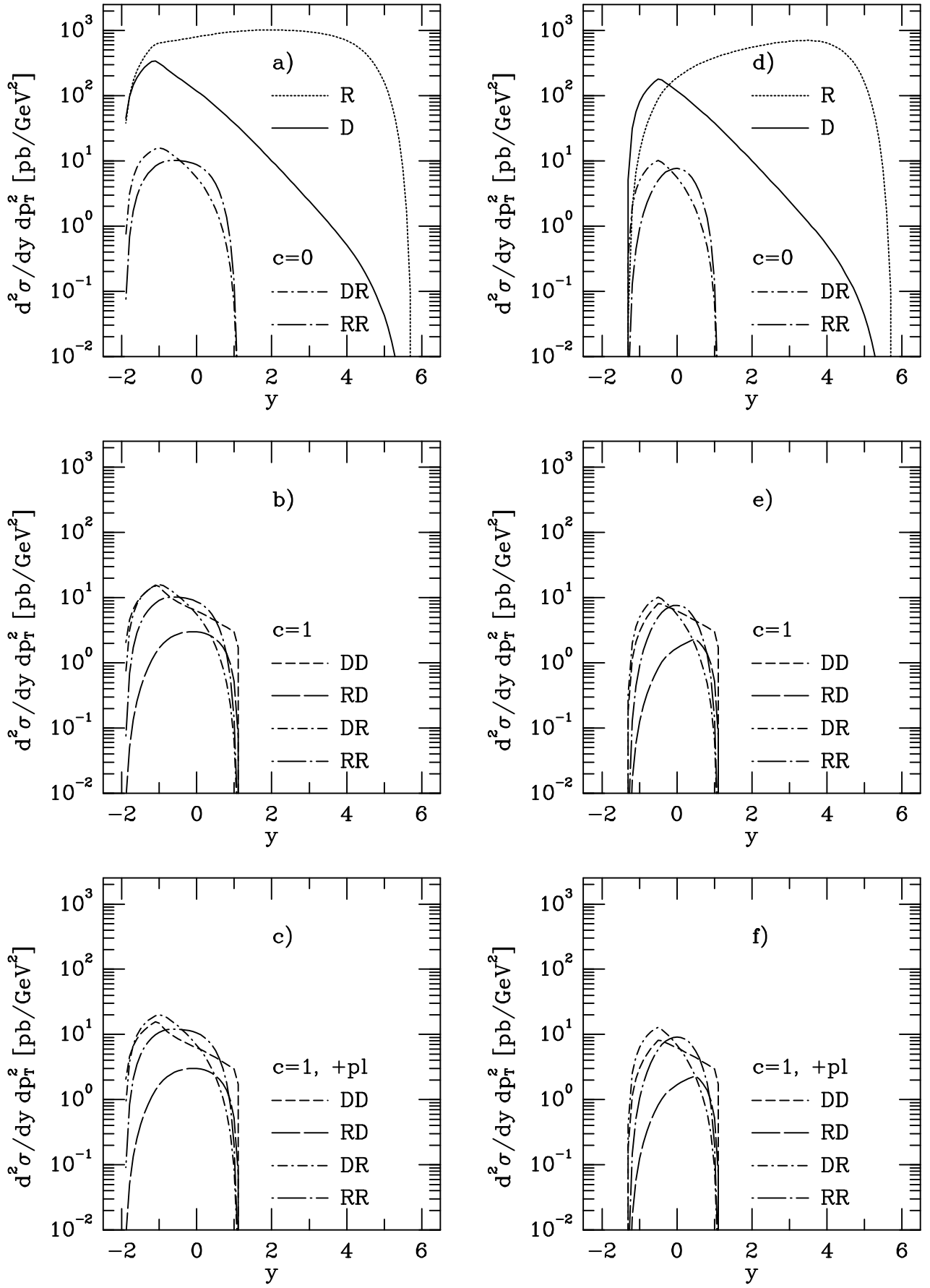


Fig. 4

This figure "fig1-5.png" is available in "png" format from:

<http://arxiv.org/ps/hep-ph/9408340v1>

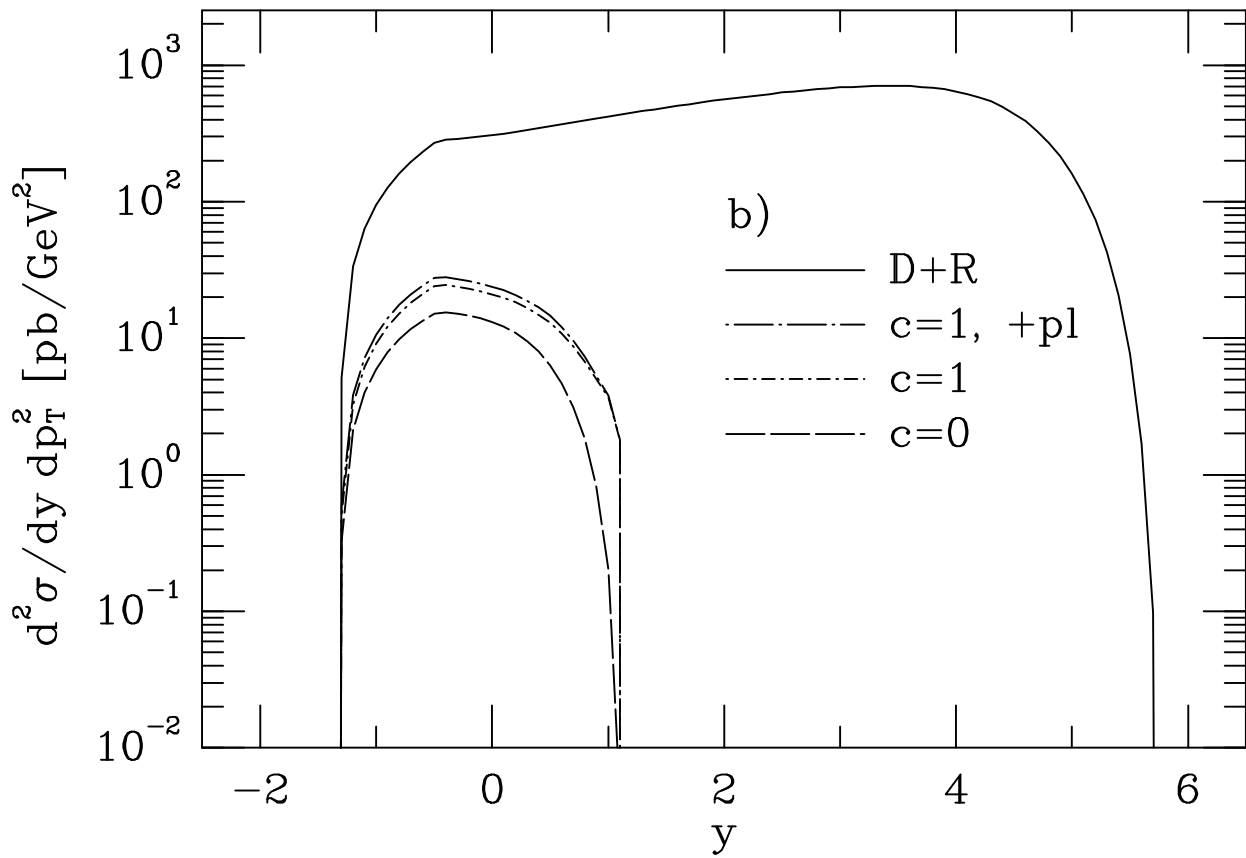
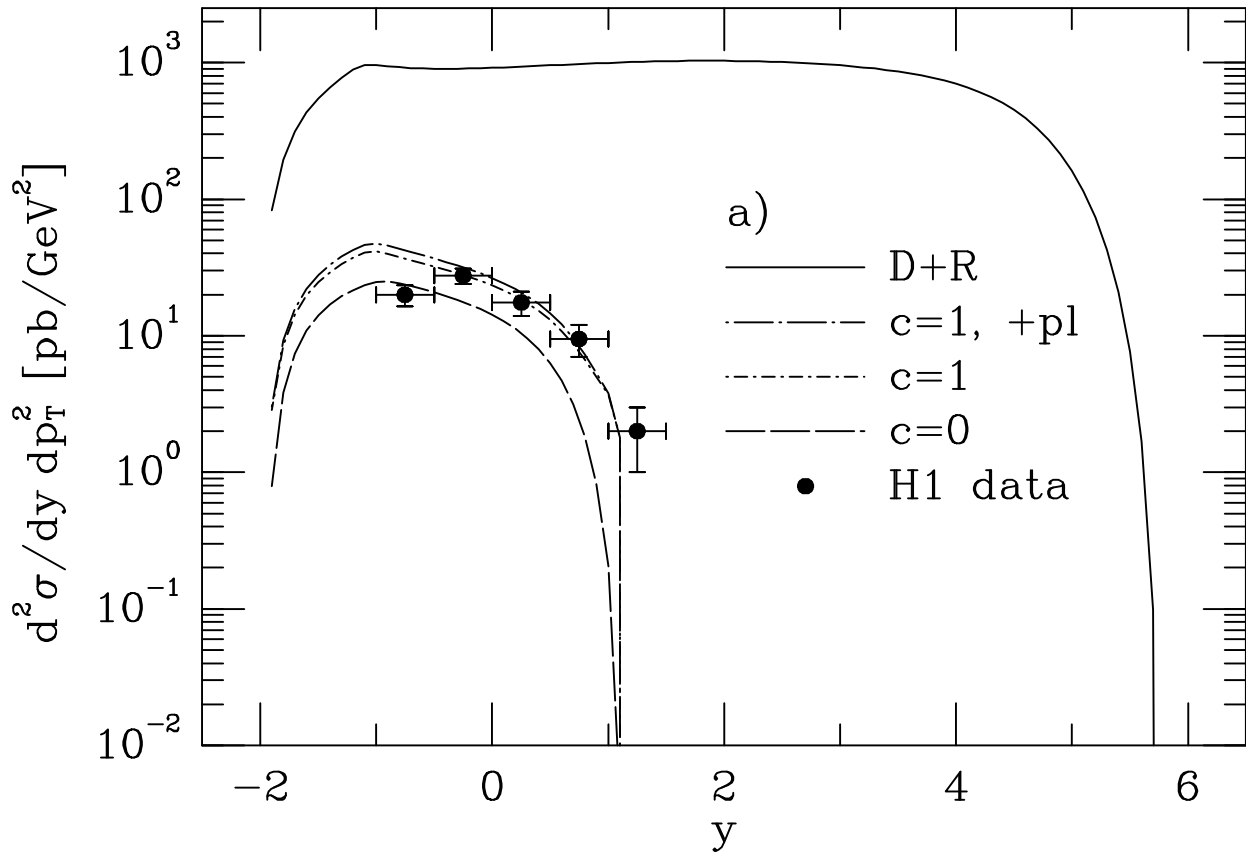


Fig. 5

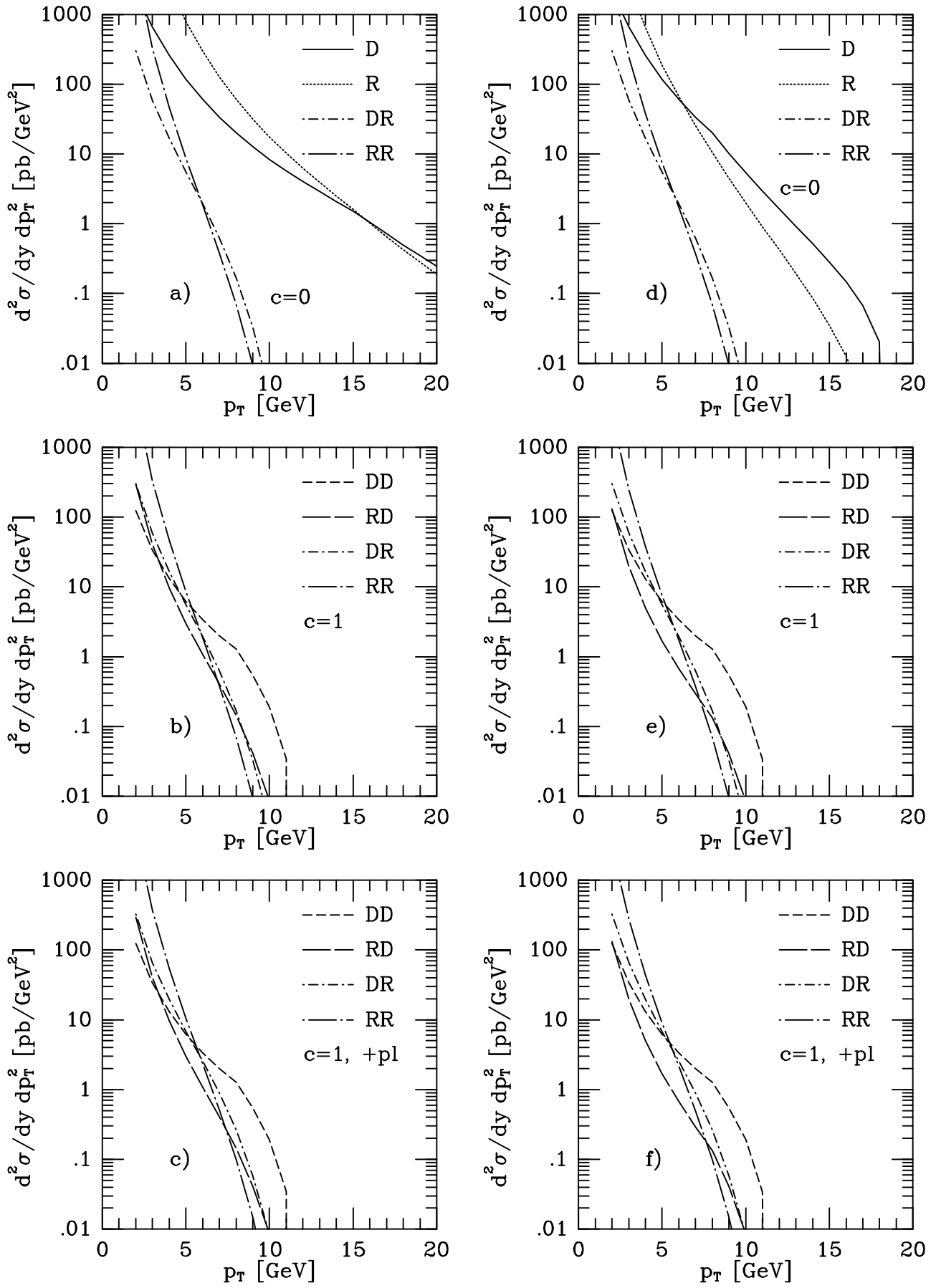


Fig. 6

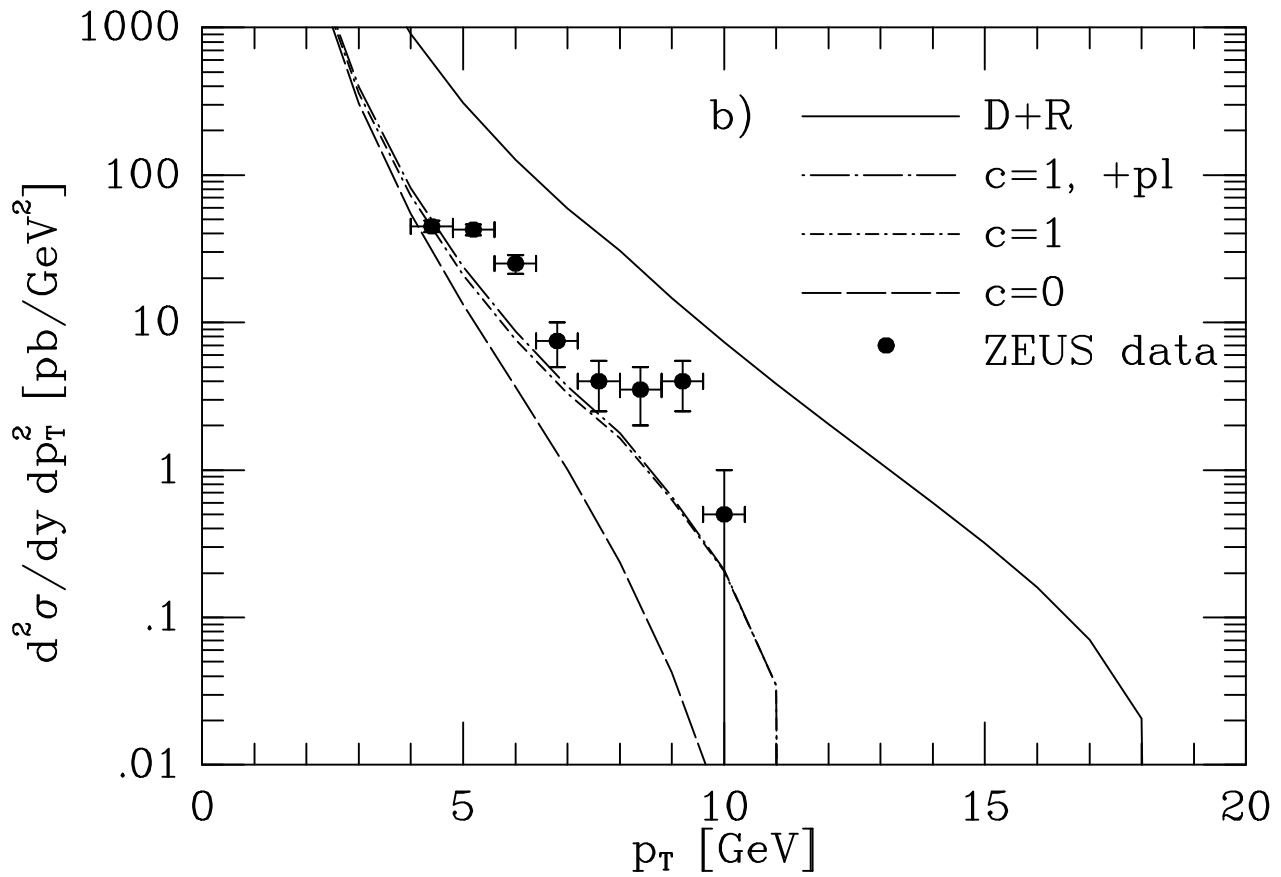
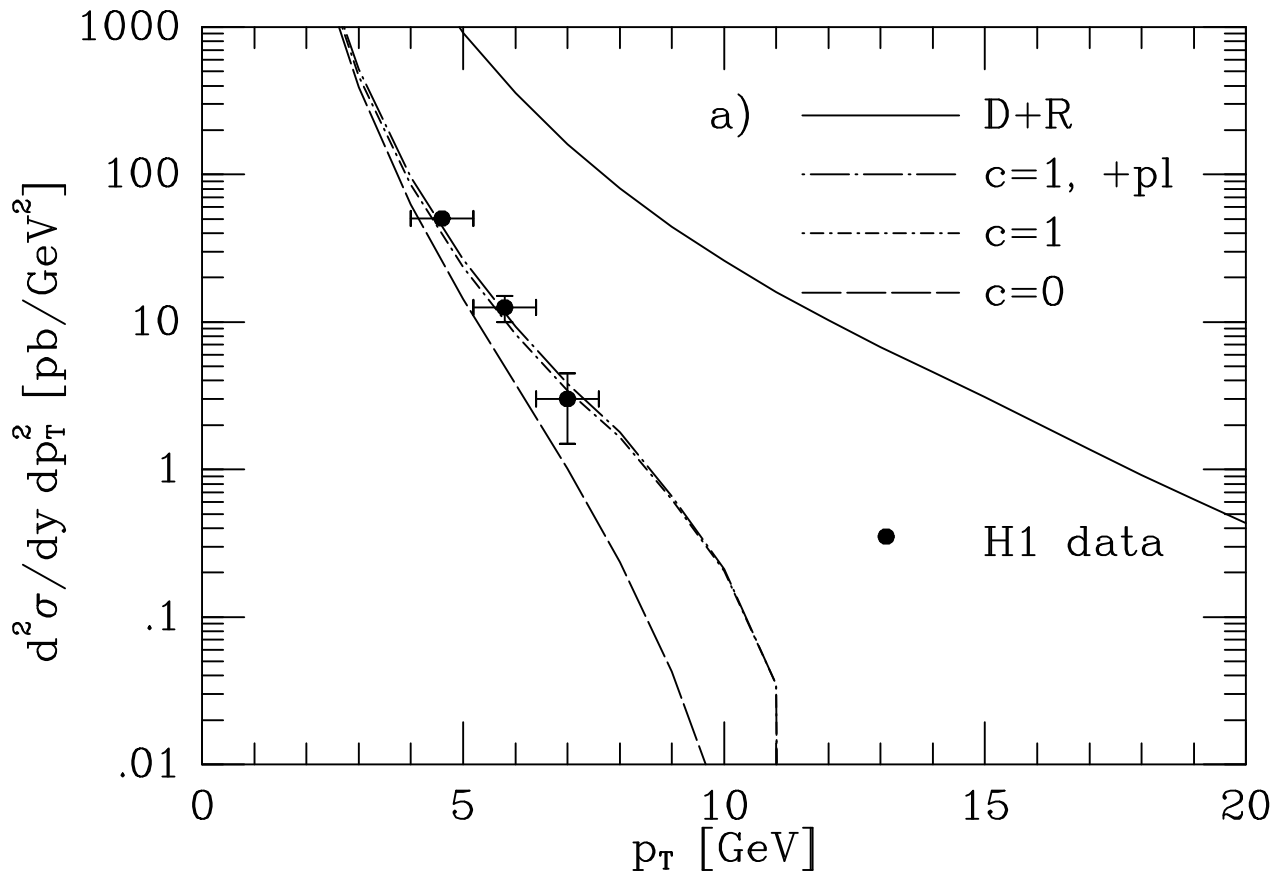


Fig. 7